Generation and Hall effect of skyrmions enabled using nonmagnetic point contacts

Zidong Wang,[1,2,*] Xichao Zhang,[3,*] Jing Xia,[3,*] Le Zhao,[1,2] Keyu Wu,[1,2] Guoqiang Yu,[4] Kang L. Wang,[5] Xiaoxi Liu,[6] Suzanne G. E. te Velthuis,[7] Axel Hoffmann,[7,†] Yan Zhou,[3] and Wanjun Jiang[1,2,‡]

[1]*State Key Laboratory of Low-Dimensional Quantum Physics and Department of Physics, Tsinghua University, Beijing 100084, China*

[2]*Frontier Science Center for Quantum Information, Tsinghua University, Beijing 100084, China*

[3]*School of Science and Engineering, The Chinese University of Hong Kong, Shenzhen, Guangdong 518172, China*

[4]*Beijing National Laboratory for Condensed Matter Physics, Institute of Physics, Chinese Academy of Sciences, Beijing 100190, China*

[5]*Department of Electrical Engineering, University of California, Los Angeles, California 90095, USA*

[6]*Department of Electrical and Computer Engineering, Shinshu University, 4-17-1 Wakasato, Nagano 380–8553, Japan*

[7]*Materials Science Division, Argonne National Laboratory, Lemont, Illinois 60439, USA*

(Received 21 April 2019; revised manuscript received 31 August 2019; published 27 November 2019)

The generation and manipulation of magnetic skyrmions are perquisites for any skyrmion-based information processing devices, where skyrmions are used as nonvolatile information carriers. In this work, we report experimentally the skyrmion generation through the usage of a nonmagnetic conducting Ti/Au point contact in a device made of a Ta/CoFeB/TaO_x trilayer film. Moreover, the accompanied topological charge-dependent skyrmion dynamics, namely the skyrmion Hall effect, is also observed in the same device. The creation process of a skyrmion has been numerically reproduced through micromagnetic simulations, in which the important role of the skyrmion-antiskyrmion pair formation is identified. The motion and Hall effect of a skyrmion, immediately after its creation, is described using a modified Thiele equation after taking into account the contribution from spatially inhomogeneous spin-orbit torques and the Magnus force. Our results on the simultaneous generation and manipulation of skyrmions using a nonmagnetic point contact are useful for understanding the ultrafast dynamics of skyrmion creation, which could also provide an effective pathway for designing skyrmion-based devices.

DOI: 10.1103/PhysRevB.100.184426

I. INTRODUCTION

Magnetic skyrmions are topological spin textures that can be found in chiral bulk magnets [1–4] and asymmetric multilayers [5–16]. In terms of potential spintronic applications, magnetic multilayers are particularly interesting not only for providing ample material systems hosting room-temperature skyrmions, but also for enabling efficient electrical manipulations through current-induced spin-orbit torques (SOTs) [8,15–20]. These asymmetric multilayers are typically made of inversion-symmetry-breaking trilayers with a perpendicular magnetic anisotropy, which contain an interfacial, noncollinear Dzyaloshinskii-Moriya interaction (DMI) [21–24] that stabilizes Néel-type skyrmions with a fixed spin chirality, in contrast to swirling Bloch-type skyrmions in most bulk chiral magnets [25]. As such, many interesting topological physics and device concepts have been revealed with direct relevance for spintronic storage and logic applications [18,26–30]. On the other hand, as skyrmions may become key components for future data storage and logic devices, electrical generation and manipulation in a controllable manner are thus essential [31,32].

The generation of magnetic skyrmions has recently been demonstrated by applying magnetic fields [8], spin-polarized currents [27,33,34], local heating [35], laser beams [36,37], and electric voltage [38,39]. Meanwhile, skyrmions can also be generated in geometrical constricted devices [6,40–44] by applying electric currents [45]. For example, the dynamical generation of skyrmions can be realized by squeezing chiral band domains through a (magnetic) geometrically constriction after being subjected to spatially inhomogeneous SOT [6,42,43,46,47]. In addition, skyrmions can also be generated in a constricted region as a result of inhomogeneous current-induced nonlinear magnetization dynamics [40,43]. Similarly, magnetic inhomogeneities with a homogeneous current may result in skyrmion nucleation [48]. However, the simultaneous occurrence of skyrmion generation and spin-topology-dependent motion–skyrmion Hall effect [11,13,44,49–51] in devices with geometrical constrictions, has not been experimentally demonstrated. The skyrmion Hall effect is important for identifying the topological nature of Néel-type skyrmions found in the related magnetic multilayers and provides a basis for enabling electrically programmable skyrmionic devices [18,52]. Early micromagnetic simulations suggested two possible regimes for skyrmion generation [46]. At low current, skyrmion nucleation may proceed via deformation of existing domain walls in a process analogous to a Rayleigh-Taylor instability [6], while larger currents may provide large enough SOTs to eliminate preexisting magnetic domain structures and nucleate new skyrmions from inhomogeneous SOTs. Since this latter mechanism does not require preexisting magnetic

*These authors contributed equally to this work.

†Present address: Department of Materials Science and Engineering, University of Illinois at Urbana-Champaign, Urbana, IL 61801, USA

‡jiang_lab@tsinghua.edu.cn

domains, we explore in this work the use of inhomogeneous current injection from a nonmagnetic point contact.

So far, it is known that the skyrmion Hall effect occurs when the translational motion of skyrmion is in the steady flow motion region, which demands a sufficiently large driving current density [6,32,53]. While typical geometrically constricted devices facilitate the formation of skyrmions, they can only tolerate a relatively small current density, above which the constriction will break [6]. In the smaller current-density region, the translational motion of skyrmion is strongly influenced by the randomly distributed pinning sites inside the materials. Namely, skyrmions stochastically hop from one pinning site to another resulting in creep motion. This explains the previous inconclusive results with respect to the skyrmion Hall effect in the devices with magnetic constrictions [6,43]. In the present work, we demonstrate the simultaneous observation of skyrmion generation and the skyrmion Hall effect in a modified Ta (5 nm)/CoFeB (1.1 nm)/TaO_x (3 nm) device with a nonmagnetic point contact. Our experimental observation is made possible by replacing the previous thin resistive magnetic geometrical constriction Ta/CoFeB/TaO_x with a conducting nonmagnetic Ti/Au point contact. The choice of a thick Ti (10 nm)/Au (100 nm) electrode allows sufficiently large electric currents that can generate skyrmions through the divergence of current-induced SOT, with less chance of the device failure and current densities sufficiently large for sustaining flow motion of the generated skyrmions. More importantly, it can also produce a steady flow motion of skyrmions together with less pronounced joule heating. It should be mentioned here that the usage of a nonmagnetic point contact excludes the generation of skyrmions inside the contact [6,40,41,43]. The location of the skyrmion generation should occur at the contact region between the constriction and ferromagnetic (FM)/heavy metal (HM)/insulator trilayer where the divergence of the current-induced SOT is maximized. It is also worth mentioning that such a skyrmion creation method using the point contact is different from that using the geometric constriction [6], where skyrmions are created based on the conversion between stripe domain walls and skyrmions, which we will discuss below.

We start to formulate the working mechanism of the proposed device, as shown in Fig. 1(a). After injecting an electron current $+j_e$ (from left to right), the constricted device naturally introduces a spatially inhomogeneous current distribution, as shown in Fig. 1(b). The convergent (left)/divergent (right) distribution of electron current density j_e in our device can be computed by solving Laplace's equations with boundary conditions of fixed potentials at the left and right ends of the device [46]. It can also be seen from Fig. 1(b) that j_e is relatively large near the contact region. It should be noted that the electrostatic potential is assumed to be constant through the thickness of the device as the thickness of the FM/HM bilayer is very thin. In addition, the FM and HM layers exhibit comparable resistivities, and the thickness of the HM layer (d_{HM}) is five times larger than that of the FM layer (d_{FM}). Thus, the electron current is mostly flowing in the HM layer. Note that the direction of electron current j_e is opposite to that of charge current j_c.

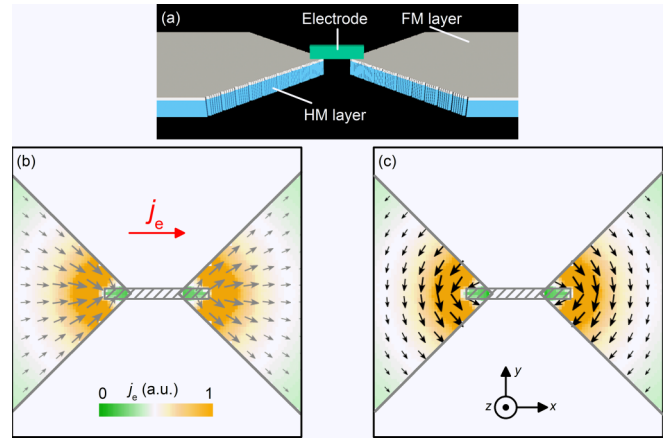

FIG. 1. (a) Schematic illustration of the geometrically constricted HM/FM heterostructure device which is connected through a nonmagnetic electrode. (b) The normalized electron-current density distribution in the HM layer. The arrow indicates the direction, and the color as well as the arrow size denote the density. (c) The corresponding spin-current density distribution in the FM layer. The arrows represent the polarization direction of spin currents. The color and arrow size represent the magnitude of spin currents.

Heavy metals exhibit a strong spin-orbit interaction that results in a spin-dependent preferential scattering, which is also known as the spin Hall effect [54,55]. Namely, in the FM/HM bilayer, a charge current is flowing in the HM layer and produces the spin current due to the spin Hall effect, which gives rise to SOT on the adjacent FM layer that can be used for manipulating the magnetization dynamics [56]. For our constricted device, the spin-current distribution j_s and its polarization for positive electron current flow is shown in Fig. 1(c), which follows the same nonuniform distribution as electron current j_e in the HM layer. It is worth mentioning that a small portion of the electron current directly flowing in the FM layer could theoretically induce magnetization dynamics through a spin-transfer torque. The contribution from spin-transfer torque to the overall skyrmion dynamics [27,46,57] has been estimated to be negligible, and therefore excluded in the present simulation.

II. RESULTS AND DISCUSSION

A. Micromagnetic simulation of skyrmion generation by using a nonmagnetic point contact

In order to reveal the feasibility of generating skyrmions using a nonmagnetic Ti/Au point contact, we first performed micromagnetic simulations by using the Object Oriented MicroMagnetic Framework (OOMMF) [58]. Following the modified Landau-Lifshitz-Gilbert equation, the magnetization dynamics driven by SOT can be written as

$$\frac{d\boldsymbol{m}}{dt} = -\gamma_0 \boldsymbol{m} \times \boldsymbol{h}_{\text{eff}} + \alpha\left(\boldsymbol{m} \times \frac{d\boldsymbol{m}}{dt}\right) - \tau_{ad}[\boldsymbol{m} \times (\boldsymbol{m} \times \boldsymbol{p})], \tag{1}$$

where t is time and α is the Gilbert damping coefficient. $\boldsymbol{h}_{\text{eff}} = -\delta\varepsilon/(\mu_0 M_S)\delta\boldsymbol{m}$ is the effective field that correlates with the functional derivative of the micromagnetic energy

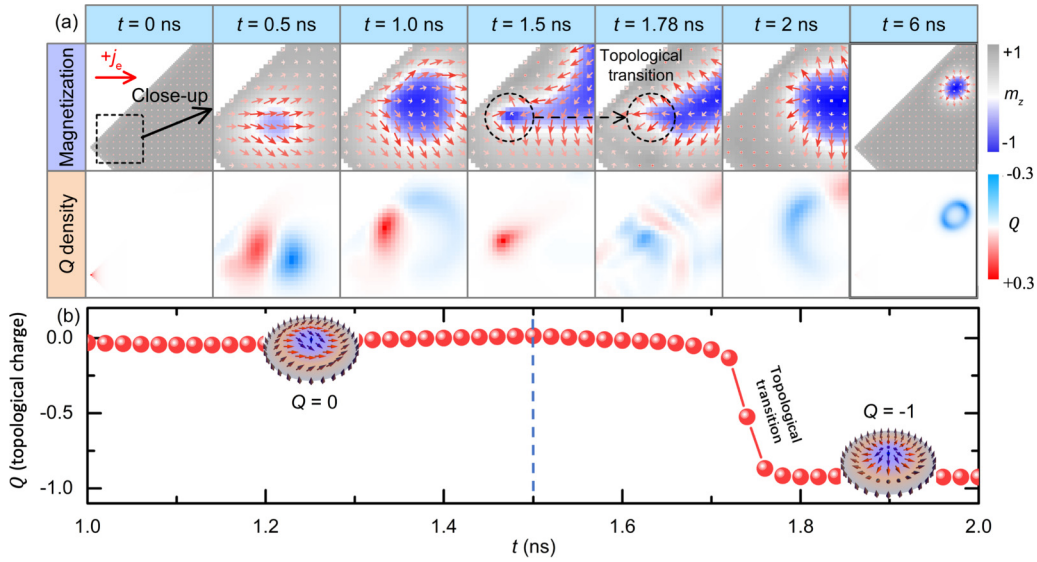

FIG. 2. Numerical demonstration of skyrmion generation enabled by inhomogeneous current-induced SOTs around the nonmagnetic contact region. (a) Evolution of magnetization profile (upper panel) and the accompanied topological charge-density profile (lower panel) as a function of time (t). In order to show the creation of skyrmions in detail, only the magnetization profiles in the region where the nucleation of skyrmion begins are shown. (b) The calculated time-dependent topological charge (i.e., the skyrmion number Q) based on the varying magnetization configurations. The dashed line at $t = 1.5$ ns indicates the switching of current from 6 to 0.03 MA cm^{-2}. The transition of topological charge from $Q = 0$ to $Q = -1$ is evident around $t = 1.7$ ns.

density ε which includes the exchange, anisotropy, Zeeman, demagnetization, and DMI terms. $\boldsymbol{m} = \boldsymbol{M}/M_S$ stands for the normalized vector of the magnetization with saturation magnetization M_S, $\boldsymbol{p}$ is the local spin-polarization direction, which is along $\hat{\boldsymbol{j}}_e \times \boldsymbol{n}$ in our device, where $\hat{\boldsymbol{j}}_e$ is the local electron current vector and $\boldsymbol{n}$ is the normal vector of the FM/HM interface. $\tau_{ad} = |\frac{\gamma_0 \hbar}{2\mu_0 e}| \frac{j_e \theta_{sh}}{d_{FM} M_S}$ represents the antidampinglike spin-torque coefficient, where γ_0 is the gyromagnetic ratio, $\hbar$ is the reduced Planck constant, μ_0 is the vacuum permeability, e is the electron charge, and d_{FM} is the thickness of the FM layer. The spin Hall angle $\theta_{sh} = j_s/j_e$ measures the conversion efficiency from charge current to spin current. Detailed discussion about micromagnetics is provided in the Supplemental Material [59]. Through micromagnetic simulation, it is found that skyrmions can be generated even in the absence of a field-like torque; we therefore only consider in the following the dominant contribution from the antidamping-like torque. The intrinsic magnetic parameters employed in our simulation are exchange stiffness $A = 10 \times 10^{-12}$ J m^{-1}, magnetic anisotropy $K = 2.89 \times 10^5$ J m^{-3} (effective anisotropy $K_{\text{eff}} = 2.34 \times 10^4$ J m^{-3}), DMI constant $D = 0.5 \times 10^{-3}$ J m^{-2}, $M_S = 6.5 \times 10^5$ A m^{-1}, $\gamma_0 = 2.211 \times 10^5$ m A^{-1} s^{-1}, $\alpha = 0.1$, and $\theta_{sk} = -0.2$. The electrical resistivities of the electrode (Au), FM layer (CoFeB), and HM layer (Ta) are set as [56]: $\rho_{Au} = 2.3 \times 10^{-8}\,\Omega$ m, $\rho_{CoFeB} = 1.7 \times 10^{-6}\,\Omega$ m, $\rho_{Ta} = 1.9 \times 10^{-6}\,\Omega$ m. The model is discretized into tetragonal cells of 5 nm × 5 nm × 1.1 nm and free tetrahedral elements with a maximum element size of 10 nm in the finite-element current-distribution calculation.

The device scheme for micromagnetic simulation mimics a device in which the HM layer, the FM layer, and nonmagnetic constricted electrode are built in a bottom-up fashion, as illustrated in Fig. 1(a). The length and width of the FM and HM layers are $l = 3000$ nm and $w = 700$ nm, respectively. The nonmagnetic electrode with a length of $l_E = 200$ nm and a width of $w_E = 20$ nm is placed at the top center of the device, bridging the left and right halves of the FM layer. The thicknesses of the HM layer, FM layer, and electrode are equal to $d_{HM} = 5$ nm, $d_{FM} = 1.1$ nm, and $d_E = 5$ nm, respectively. In the micromagnetic simulation, the skyrmion may be destructed by touching the sample edges. To display the nucleation of skyrmions completely, the magnetizations of the cells along the edge of the FM layer are fixed to the initial relaxed direction to prevent the destruction of skyrmions due to the skyrmion Hall effect. In order to reveal the topological properties of the generated magnetization textures, we have also calculated the evolution of the topological charge based on the magnetization configuration simulated by oommf. The topological charge of spin textures, namely, the skyrmion number, is expressed as $Q = {}^1/_{4\pi} \int \boldsymbol{m} \cdot ({}^{\partial \boldsymbol{m}}/_{\partial x} \times {}^{\partial \boldsymbol{m}}/_{\partial y}) dxdy$. A well-defined ground-state skyrmion has a skyrmion number of $|Q| = 1$.

The numerical demonstration of the generation process of a single isolated skyrmion is enabled by using the spatially divergent antidampinglike SOT near the contact region. The electron current pulse is $j_e = 6$ MA cm^{-2} that is normalized by the width of the wider part of device $w = 700$ nm. Figure 2(a) illustrates the complete generation process of an isolated $Q = -1$ skyrmion, where the upper and lower panels show, respectively, the detailed evolutions of magnetization configurations and the associated topological charge densities [i.e., $q(t) = \boldsymbol{m} \cdot ({}^{\partial \boldsymbol{m}}/_{\partial x} \times {}^{\partial \boldsymbol{m}}/_{\partial y})$] as a function of time (t). It is clear that in the topological charge of the magnetization configuration there exists a transition from a topologically trivial bubble with $Q = 0$ to a topologically nontrivial skyrmion with

$Q = -1$ [Fig. 2(b)]. In the first $t = 0{\sim}0.5$ ns (immediately after applying a current), the magnetization orientation near the contact region between constriction and trilayer reverses from upward to downward and forms a circular bubble domain with a substantial in-plane magnetization component aligned along the $+x$ direction. The associated topological charge can be calculated as $Q = 0$. This topologically trivial magnetic bubble continues to expand and moves into a wider area of the FM layer driven by the spatially divergent current-induced SOT, while $t = 0.5{\sim}1.0$ ns.

During $t = 1.0{\sim}1.5$ ns, the in-plane magnetization component of the circular bubble domain rotates and evolves from a quasiuniform configuration pointing along the $+x$ direction into an outward-pointing configuration favored by the interface-induced DMI, where an intriguing defectlike magnetization texture is formed at the left side of the bubble, as indicated by the dashed circle in Fig. 2(a) at $t = 1.5$ ns. Such a defectlike magnetization texture has an associated topological charge of $Q \sim +1$, which means that it can be regarded as an antiskyrmion excitation [60,61]. On the other hand, the other larger part of the bubble has an associated topological charge of $Q \sim -1$, indicating a skyrmion excitation is also formed at the same time. Namely, the total skyrmion number of the FM layer still remains at $Q = 0$. We note that the excitation of such a skyrmion-antiskyrmion pair from a bubble with $Q = 0$ is due to the topological conservation, since a continuous transformation and deformation of magnetization texture are processed at the current stage.

In order to avoid generation of extra skyrmions under the large current density that complicates the subsequent analysis, after $t = 1.5$ ns, j_e is reduced to be $0.03\,\mathrm{MA\,cm^{-2}}$. This current density is unable to switch magnetization in the vicinity of the point contact, but can further drive the motion of the existing $Q = 0$ topologically trivial bubble, which would transform into an elongated shape. Following the expansion of the bubble domain, the size of the $Q = +1$ antiskyrmion reduces accordingly. The reason is that the antiskyrmion texture is energetically unstable in the presence of the isotropic interfacial DMI in the system [60,61]. When the antiskyrmion shrinks to the lattice size, the antiparallel magnetization configuration abruptly switches to be parallel, namely, the antiskyrmion is annihilated at $t = 1.78$ ns. It is noteworthy mentioning that spin waves are excited and emitted from the position where the antiskyrmion is annihilated that results in energy dissipation in the FM layer, which can be discerned from the propagating skyrmion number density wave at $t = 1.78$ ns. The annihilation process is due to the fact that the antiskyrmion is an unstable elementary excitation in the given FM system with isotropic DMI [60,61], which will shrink and collapse as a function of time due to Gilbert damping [62]. It is worth mentioning that the antiskyrmion textures with $Q = +1$ can be stabilized by anisotropic DMI [61] frustrated exchange interactions [63], while the DMI in our device is of interface-induced isotropic form and only stabilizes skyrmions with $Q = -1$.

Once the antiskyrmion is annihilated, the remained elongated bubble domain has a circular domain wall with an outward-pointing configuration at $t = 2$ ns, and the topological charge of the remained elongated bubble domain can be calculated as $Q = -1$, which means it is a stable Néel-type $Q = -1$ skyrmion. Subsequently, the created Néel-type skyrmion with $Q = -1$ continues to move into a wide area of the FM layer, and eventually shrinks to an energy-favorable circular shape ($t = 6$ ns). Therefore, it can be seen that the transition of topological charge of magnetic texture from being a topologically trivial bubble with $Q = 0$ to a topologically nontrivial skyrmion with $Q = -1$ in the FM layer is thus mediated by the creation of a skyrmion-antiskyrmion pair and the subsequent annihilation of the antiskyrmion, which is similar to the case in Ref. [48].

Figure 2(b) illustrates the topological transition process of $Q = 0 \rightarrow Q = -1$. As discussed above, the creation of a stable $Q = -1$ skyrmion in the given FM system is mediated by the creation and annihilation of an unstable $Q = +1$ antiskyrmion [see Fig. 2(b) insets]. It means that a skyrmion-antiskyrmion pair is actually created during the magnetization switching process, obeying the topological conservation law. However, as the $Q = +1$ antiskyrmion is an energy-unfavorable solution, it decays and annihilates once it is created, while the $Q = -1$ skyrmion, once it is created, is a stable solution stabilized by the interface-induced DMI. As mentioned above, the annihilation of the unstable $Q = +1$ antiskyrmion will excite a bunch of propagating spin waves, which means that the local energy carried by the $Q = +1$ antiskyrmion is globally dissipated in the FM layer.

Figure 3 shows the time evolution of skyrmion number Q and all micromagnetic energies during the skyrmion creation process. When the electron current pulse is applied for $t = 0 \sim 1.5$ ns, the magnetization underneath the point contact is reversed by the spatially divergent current-induced SOT, forming a $Q = 0$ bubble. It can be seen that the total micromagnetic energy, anisotropy energy, and demagnetization energy significantly oscillate during this period due to the magnetization rotation of the bubble structure. The exchange energy increases with increasing time, which is caused by the formation and elongation of domain wall. Because of the same reason, the DMI energy decreases with increasing time. When the electron current pulse is terminated at $t = 1.5$ ns, the oscillation of the total micromagnetic energy, anisotropy energy, and demagnetization energy suddenly stops. Meanwhile, the exchange energy and DMI energy show a sharp increase and decrease, respectively. The reason is that the magnetization in the bubble domain wall stops rotating, while a $Q = -1$ antiskyrmion with antiparallel magnetization configuration is generated. In a very short period, the antiskyrmion is annihilated, resulting in the creation of the $Q = -1$ skyrmion in the FM layer. The exchange energy shows a sharp decrease corresponding to the annihilation of the antiskyrmion. When the skyrmion is created, it moves in the FM layer driven by SOT. Hence, the total micromagnetic energy of the system further decreases and approaches a stable value, indicating the stability of the system.

Note that in our micromagnetic simulation, the influence of defects is not considered. However, it should be noted that it has also been shown that magnetic defects can give rise to a skyrmion-antiskyrmion generation, which subsequently due to their opposite gyrotropic Magnus forces separate laterally [48]. In this instance, DMI can also favor the stability of one (i.e., skyrmions) over the other (i.e., antiskyrmions).

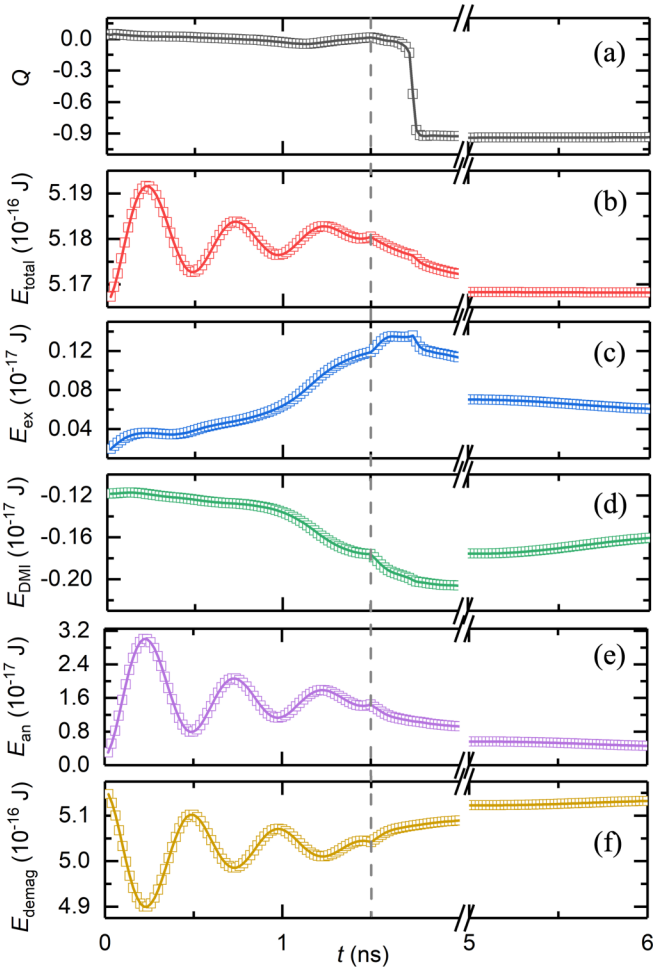

FIG. 3. Time evolution of (a) skyrmion number Q, (b) total micromagnetic energy E_{total}, (c) exchange energy E_{ex}, (d) DMI energy E_{DMI}, (e) anisotropy energy E_{an}, and (f) demagnetization energy E_{demag} in the skyrmion creation process.

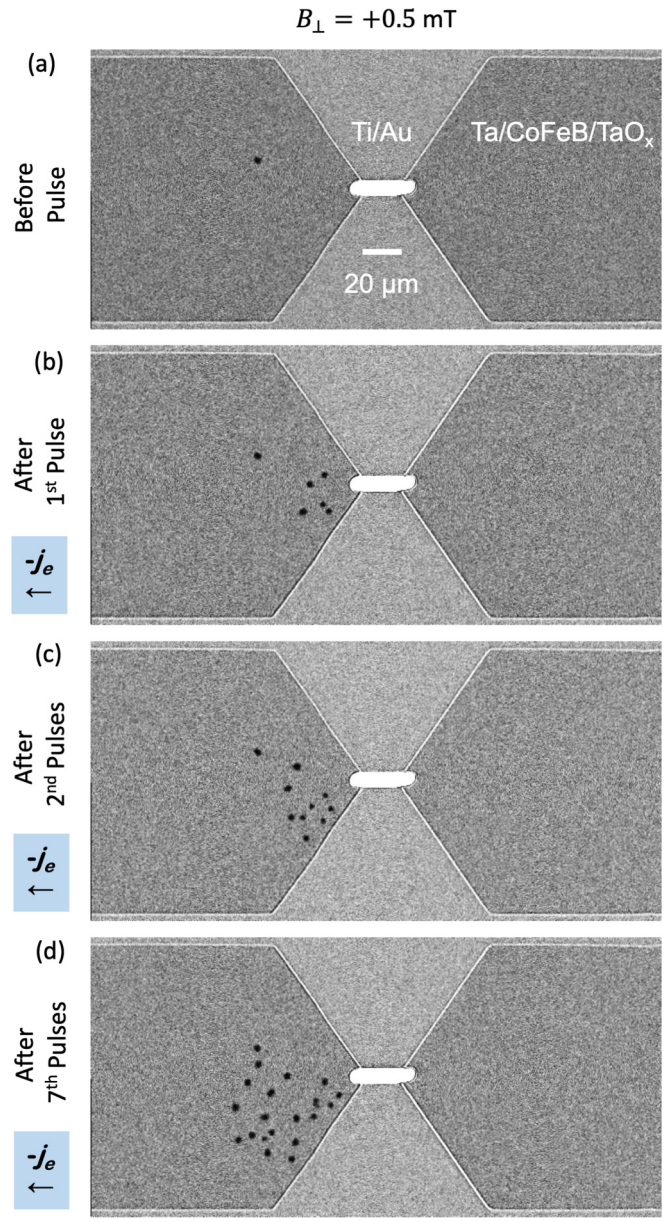

FIG. 4. Sequential MOKE images driven by a train of voltage pulses showing continuous creation and the subsequent accumulation of skyrmions at lower side of the device, namely, the occurrence of skyrmion Hall effect. The experiment was performed under a perpendicular magnetic field $B_\perp = +0.5$ mT. The applied voltage pulses are of +15 V in amplitude and 1 ms in duration.

B. Experimental generation of skyrmion via nonmagnetic point contact

We have numerically discussed the feasibility of generating skyrmions underneath a nonmagnetic contact in the presence of inhomogeneous SOTs. Below we will realize it experimentally in a device made of a Ta(5 nm)/$Co_{20}Fe_{60}B_{20}$(1.1 nm)/TaO_x(3 nm) trilayer and a nonmagnetic point contact of Ti (10 nm)/Au (100 nm) as is shown in the schematic in Fig. 1(a). The multilayer was grown by ultrahigh vacuum magnetron sputtering and patterned via standard photolithography and ion milling. The nonmagnetic Ti/Au constriction is of length 20 μm and of width 4 μm which were made following a lift-off process. A polar magneto-optical Kerr effect (MOKE) microscopy was used for imaging the magnetic domain patterns. For all images presented, a background image is subtracted. The background image is taken while applying a sufficiently large field to magnetically saturate the sample.

Figure 4 shows the creation and the subsequent translational motion of magnetic skyrmions. In the presence of a perpendicular magnetic field of $B_\perp = +0.5$ mT, only one isolated skyrmion bubble on the left side of the Ti/Au constriction can be seen. The magnetization on the right side of the trilayer remains in a positive saturation state, as shown in Fig. 4(a). On the other hand, after passing a positive voltage pulse of amplitude 15 V (from left to right) and of duration 1 ms through the device, the generation of skyrmion bubbles is evident on the right side of Ti/Au constriction, as shown in Figs. 4(b)–4(d). The corresponding current density in the Ti/Au constriction is computed as 8.8 MA cm^{-2} by measuring the resistance of device ($R = 3.86$ kΩ), a current density that is comparable with the one used in micromagnetic simulation. It is noted that the direction of the electron

current is determined by the applied voltage. The location of the skyrmion formation coincides with the contact region between the Ti/Au electrode and magnetic multilayer at which the divergent electron current and hence divergent SOTs are the largest. It is thus conceivable that the divergence of SOTs is critical for triggering magnetization instabilities that help to form magnetic skyrmions [40,64]. After applying the pulse, the magnetization configuration on the right side of the device, however, remains the same as before. While the generation process of skyrmion bubbles can be understood based on the above micromagnetic simulation, the details cannot be experimentally identified here due to limitations in both the temporal and spatial resolution of the MOKE microscope. These skyrmion bubbles, once generated, bear a translational motion as a result of both inhomogeneous SOT and gyrotropic Magnus force. Furthermore, upon applying consecutive voltage pulses, many additional skyrmion bubbles were generated and move into the wider area that indicates the reproducibility of the generation. This leads to the accumulation of skyrmions on the lower left part of the device, consistent with the skyrmion Hall effect. Note that we also computationally studied the same phenomenon by using micromagnetic simulations, of which the results are in line with our experimental observations.

It is known that the Magnus force can result in a skyrmion Hall effect and skyrmion accumulation in the presence of homogeneous SOTs [50,65]. The present system, however, also involves contribution from the inhomogeneous current-induced SOTs [11,13]. In order to elucidate whether the origin of skyrmion accumulation is from the Magnus force or from the spatially inhomogeneous SOTs, below we adopted a modified Thiele equation to analyze the dynamics of the magnetic skyrmion, as expressed below [11,29,32,66,67]:

$$\boldsymbol{\mathcal{G}} \times \boldsymbol{v} - \alpha \boldsymbol{\mathcal{D}} \cdot \boldsymbol{v} - 4\pi \boldsymbol{\mathcal{B}} \cdot \boldsymbol{j}_{\mathrm{e}} = \boldsymbol{0}, \tag{2}$$

where the first term describes the Magnus force which results in the transverse motion of skyrmions with respect to the injected electron current $\boldsymbol{j}_{\mathrm{e}}$, $\mathcal{G} = (0, 0, -4\pi Q)$ is the gyromagnetic coupling vector, and $\boldsymbol{v} = (v_x, v_y)$ is the drift velocity of the skyrmion. Note that the sign of the gyrotropic Magnus force is determined by both the sign of topological charge (Q) and the direction of motion of skyrmion ($\boldsymbol{v}$). The second term describes the dissipative force with the dissipative tensor $\mathcal{D}$ describing the effect of the drag force on the moving skyrmion $\boldsymbol{\mathcal{D}} = 4\pi \begin{pmatrix} \mathcal{D}_{xx} & \mathcal{D}_{xy} \\ \mathcal{D}_{yx} & \mathcal{D}_{yy} \end{pmatrix}$. For a rigid Néel-type skyrmion (no distortion during motion), relations between each component are $\mathcal{D}_{xx} = \mathcal{D}_{yy} = \mathcal{D}$ and $\mathcal{D}_{xy} = \mathcal{D}_{yx} = 0$, and the value of $\mathcal{D} = \pi^2 d/8\gamma_{dw}$ can be estimated based on the skyrmion profile [11], where d is the diameter of the skyrmion and γ_{dw} is the domain wall width. The third term is the driving force provided by current-induced SOT with $\boldsymbol{j}_{\mathrm{e}} = (j_x, j_y)$ and $\boldsymbol{\mathcal{B}} = \frac{\tau_{\mathrm{ad}}}{j_{\mathrm{e}}} \begin{pmatrix} -\mathcal{J}_{xy} & \mathcal{J}_{xx} \\ -\mathcal{J}_{yy} & \mathcal{J}_{yx} \end{pmatrix}$ that quantifies the efficiency of the SOTs over the skyrmion bubbles. The components are given as $\mathcal{J}_{\mu\nu} = \frac{1}{4\pi} \int (\frac{\partial \boldsymbol{m}}{\partial \mu} \times \boldsymbol{m})_{\nu} dxdy$, where μ and υ run over x and y. For the rigid hedgehoglike skyrmion, the relations that hold are $\mathcal{J}_{xx} = \mathcal{J}_{yy} = 0$ and $\mathcal{J}_{xy} = -\mathcal{J}_{yx} = \mathcal{J}$.

In our constricted device geometry, the current distribution (j_x, j_y) can be computed by using Laplace's equation [42,46]. After solving Eq. (2), we obtain the projection of the skyrmion velocities along the x and y directions as follows:

$$v_x = \left| \frac{\tau_{\mathrm{ad}}}{j_{\mathrm{e}}} \right| \mathcal{J} \frac{\alpha \mathcal{D} j_x + Q j_y}{Q^2 + \alpha^2 \mathcal{D}^2} \quad \text{and} \quad v_y = \left| \frac{\tau_{ad}}{j_{\mathrm{e}}} \right| \mathcal{J} \frac{\alpha \mathcal{D} j_y - Q j_x}{Q^2 + \alpha^2 \mathcal{D}^2}. \tag{3}$$

By defining a skyrmion Hall angle $\tan\Phi_{\mathrm{sk}} = {}^{v_y}/_{v_x}$, it is found that

$$\tan\Phi_{\mathrm{sk}} = \frac{\alpha \mathcal{D} j_y - Q j_x}{\alpha \mathcal{D} j_x + Q j_y}. \tag{4}$$

Note that Eq (4) can be further simplified as $\Phi_{\mathrm{sk}} = -Q/\alpha\mathcal{D}$ when the driving currents (SOTs) are homogeneous as has been previously used for quantifying the skyrmion Hall effect in various multilayers [11,13].

From Eq. (4), it is clear that both the inhomogeneous current distribution (j_x, j_y), the value of $\alpha\mathcal{D}$, and the topological charge of the skyrmion ($Q = \pm 1$) could influence the magnitude of skyrmion Hall angle. In the following, we will examine the contribution from each component individually. For the given material-specific parameters, the domain-wall widths can be calculated as $\gamma_{\mathrm{dw}} = \pi\sqrt{\mathcal{A}/K_{\mathrm{eff}}} \approx 63$ nm that leads to the value of $\mathcal{D} = \pi^2 d/8\gamma_{\mathrm{dw}}$ to be determined as $\mathcal{D} \approx 20$. For the Ta/CoFeB/TaO_x trilayer, the magnetic damping parameter is $\alpha \approx 0.02$. The value of $\alpha\mathcal{D}$ is estimated to be $\approx 0.4 < 1$. For the given triangular geometry, the current distribution j_y/j_x around the contact region is about 1. Thus, the sign of skyrmion Hall angle is predominantly controlled by the sign of topological charge Q.

As indicated by Eq. (4), the sign of the gyrotropic Magnus force ($\boldsymbol{\mathcal{G}} \times \boldsymbol{v}$) is governed by both the sign of topological charge ($Q = \pm 1$) and the direction of skyrmion motion ($\boldsymbol{v}$). The sign of topological charge can be reversed upon changing the polarity of the perpendicular magnetic fields since Q is an odd function of magnetization vector $\boldsymbol{m}$. The direction of skyrmion motion, after moving away from the constricted region, is controlled solely by the (electron) current along the horizontal direction ($\pm x$). This enables a diagram of the skyrmion Hall effect as a function of topological charge ($\pm Q$) and driving currents ($\pm j_{\mathrm{e}}$) to be established, as shown in Fig. 5. By reversing the current/field directions, we can clearly see that the location of skyrmion accumulation is changed accordingly in our symmetrically designed device. In addition, the position of skyrmion generation is consistent with the position where the divergence of SOTs is maximized. When the polarity of (electron) current pulse is fixed along the $-x$ direction (i.e., $-j_{\mathrm{e}}$), the position of skyrmion accumulation reverses from the top to the bottom of the left side of the device after changing the perpendicular magnetic field from $B_{\perp} = -0.5$ mT to $B_{\perp} = +0.5$ mT. This is again consistent with the fact that the topological Magnus force changes its sign upon reversal of magnetic field (from $Q = +1$ to $Q = -1$). By reversing the polarity of (electron) current pulse to the $+x$ direction (i.e., $+j_{\mathrm{e}}$), the location of skyrmion accumulation is being reversed. These observations are consistent with the theoretical prediction and suggest that gyrotropic Magnus forces dominate the skyrmion dynamics.

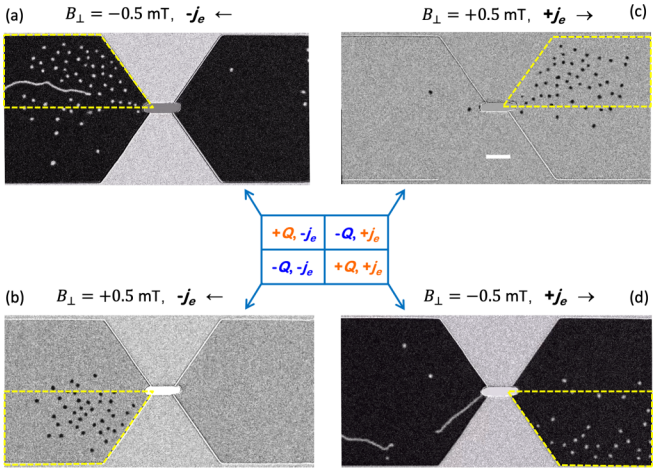

FIG. 5. A diagram of the skyrmion Hall effect for opposite sign of topological charge ($Q = \pm 1$) and opposite direction of voltage/current polarity ($\pm j_e$). (a) $-j_e$ flows toward the $-x$ direction with $Q = +1$ ($B_\perp = -0.5$ mT). (b) $-j_e$ flows toward the $-x$ direction with $Q = -1$ ($B_\perp = +0.5$ mT). (c) $+j_e$ flows toward the $+x$ direction with $Q = -1$ ($B_\perp = +0.5$ mT). (d) j_e flows toward the $+x$ direction with $Q = +1$ ($B_\perp = -0.5$ mT). These images were taken after applying 20 pulses of +15 V in amplitude and 1 ms in duration. Scale bar corresponds to 20 μm.

III. CONCLUSION

In summary, we have numerically and experimentally studied the generation of magnetic skyrmions in a Ta/CoFeB/TaO_x trilayer together with a nonmagnetic Ti/Au point contact. The topological transition of spin textures from being a topologically trivial bubble $Q = 0$ to a topologically nontrivial skyrmion $Q = -1$ is clearly resolved in micromagnetic simulations. These simulations also show the important role of the formation of a skyrmion-antiskyrmion pair and the subsequent annihilation of the antiskyrmion in forming an isolated individual skyrmion. The formation of the skyrmion-antiskyrmion pair is guaranteed by the topological conservation, while the antiskyrmion annihilation is due to the presence of the interface-induced isotropic DMI in our device, which only stabilizes the Néel-type skyrmions. Experimentally, in the device with a nonmagnetic point contact, we show skyrmions can be dynamically generated near the contact region. The skyrmion formation is directly related to the spatially divergent inhomogeneous current-induced SOT. We note that such a skyrmion generation mechanism is different from that reported in Ref. [6], where the skyrmion is created based on the conversion between stripe domain walls and skyrmions. Since a nonmagnetic conducting Ti/Au electrode allows sufficient electric current to flow through, we further observed the spin-topology-driven skyrmion dynamics, *i.e.*, the skyrmion Hall effect. The observation of the skyrmion Hall effect can be well described by a modified Thiele equation in the presence of spatially divergent SOT. Our results could provide useful information for manipulating magnetic skyrmions in a controllable manner and for designing functional skyrmion devices that are based on the unique topological charge of magnetization textures.

ACKNOWLEDGMENTS

Work carried out at Tsinghua University was supported by the Basic Science Center Project of NSFC (Grant No. 51788104), National Key R&D Program of China (Grants No. 2017YFA0206200 and No. 2016YFA0302300), the NSFC Grants No. 11774194, No. 51831005, and No. 1181101082, Beijing Natural Science Foundation (Grant No. Z19J00024), Tsinghua University Initiative Scientific Research Program and the Beijing Advanced Innovation Center for Future Chip (ICFC). X.Z. acknowledges the support by the Presidential Postdoctoral Fellowship of The Chinese University of Hong Kong, Shenzhen (CUHKSZ). Y.Z. acknowledges the support by the President's Fund of CUHKSZ, Longgang Key Laboratory of Applied Spintronics, National Natural Science Foundation of China (Grants No. 11974298 and No. 61961136006), Shenzhen Fundamental Research Fund (Grant No. JCYJ20170410171958839), and Shenzhen Peacock Group Plan (Grant No. KQTD20180413181702403). X.L. acknowledges the support by the Grants-in-Aid for Scientific Research from JSPS KAKENHI (Grants No. 17K19074, No. 26600041, and No. 22360122). Work carried out at the Argonne National Laboratory (lithography, MOKE imaging, and Ti/Au deposition) was supported by the U.S. Department of Energy, Office of Science, Basic Energy Science, Materials Science and Engineering Division.

[1] U. K. Rossler, A. N. Bogdanov, and C. Pfleiderer, Spontaneous skyrmion ground states in magnetic metals, Nature (London) **442**, 797 (2006).

[2] S. Mühlbauer, B. Binz, F. Jonietz, C. Pfleiderer, A. Rosch, A. Neubauer, R. Georgii, and P. Böni, Skyrmion lattice in a chiral magnet, Science **323**, 915 (2009).

[3] X. Z. Yu, Y. Onose, N. Kanazawa, J. H. Park, J. H. Han, Y. Matsui, N. Nagaosa, and Y. Tokura, Real-space observation of a two-dimensional skyrmion crystal, Nature (London) **465**, 901 (2010).

[4] N. Nagaosa and Y. Tokura, Topological properties and dynamics of magnetic skyrmions, Nat. Nanotechnol. **8**, 899 (2013).

[5] F. Büttner, C. Moutafis, M. Schneider, B. Krüger, C. M. Günther, J. Geilhufe, C. V. Schmising, J. Mohanty, B. Pfau, S. Schaffert, A. Bisig, M. Foerster, T. Schulz, C. A. F. Vaz, J. H. Franken, H. J. M. Swagten, M. Kläui, and S. Eisebitt, Dynamics and inertia of skyrmionic spin structures, Nat. Phys. **11**, 225 (2015).

[6] W. Jiang, P. Upadhyaya, W. Zhang, G. Yu, M. B. Jungfleisch, F. Y. Fradin, J. E. Pearson, Y. Tserkovnyak, K. L. Wang, O. Heinonen, S. G. E. te Velthuis, and A. Hoffmann, Blowing magnetic skyrmion bubbles, Science **349**, 283 (2015).

[7] G. Chen, A. Mascaraque, A. T. N'Diaye, and A. K. Schmid, Room temperature skyrmion ground state stabilized through

interlayer exchange coupling, Appl. Phys. Lett. **106**, 242404 (2015).

[8] S. Woo, K. Litzius, B. Kruger, M. Y. Im, L. Caretta, K. Richter, M. Mann, A. Krone, R. M. Reeve, M. Weigand, P. Agrawal, I. Lemesh, M. A. Mawass, P. Fischer, M. Kläui, and G. S. Beach, Observation of room-temperature magnetic skyrmions and their current-driven dynamics in ultrathin metallic ferromagnets, Nat. Mater. **15**, 501 (2016).

[9] C. Moreau-Luchaire, S. C. Mouta, N. Reyren, J. Sampaio, C. A. Vaz, N. Van Horne, K. Bouzehouane, K. Garcia, C. Deranlot, P. Warnicke, P. Wohlhuter, J. M. George, M. Weigand, J. Raabe, V. Cros, and A. Fert, Additive interfacial chiral interaction in multilayers for stabilization of small individual skyrmions at room temperature, Nat. Nanotechnol. **11**, 444 (2016).

[10] O. Boulle, J. Vogel, H. Yang, S. Pizzini, D. de Souza Chaves, A. Locatelli, T. O. Mentes, A. Sala, L. D. Buda-Prejbeanu, O. Klein, M. Belmeguenai, Y. Roussigne, A. Stashkevich, S. M. Cherif, L. Aballe, M. Foerster, M. Chshiev, S. Auffret, I. M. Miron, and G. Gaudin, Room-temperature chiral magnetic skyrmions in ultrathin magnetic nanostructures, Nat. Nanotechnol. **11**, 449 (2016).

[11] W. Jiang, Z. Xichao, G. Yu, W. Zhang, X. Wang, M. B. Jungfleisch, J. E. Pearson, X. Cheng, O. Heinonen, K. L. Wang, Y. Zhou, A. Hoffmann, and S. G. E. te Velthuis, Direct observation of the skyrmion Hall effect, Nat. Phys. **13**, 162 (2017).

[12] W. Jiang, G. Chen, L. Kai, Z. Jiadong, G. E. t. V. Suzanne, and H. Axel, Skyrmions in magnetic multilayers, Phys. Rep. **704**, 1 (2017).

[13] K. Litzius, I. Lemesh, B. Krüger, P. Bassirian, L. Caretta, K. Richter, F. Büttner, K. Sato, O. A. Tretiakov, J. Förster, R. M. Reeve, M. Weigand, I. Bykova, H. Stoll, G. Schütz, G. S. D. Beach, and M. Kläui, Skyrmion Hall effect revealed by direct time-resolved x-ray microscopy, Nat. Phys. **13**, 170 (2017).

[14] A. Soumyanarayanan, M. Raju, A. L. Gonzalez Oyarce, A. K.C. Tan, M.-Y. Im, A. P. Petrovic, P. Ho, K .H. Khoo, M. Tran, C. K. Gan, F. Ernult, and C. Panagopoulos, Analogue tuning of magnetic skyrmion properties at room temperature in Ir/Fe/Co/Pt multilayers, Nat. Mater. **16**, 898 (2017).

[15] A. Fert, N. Reyren, and V. Cros, Magnetic skyrmions: advances in physics and potential applications, Nat. Rev. Mater. **2**, 17031 (2017).

[16] F. Hellman, A. Hoffmann, Y. Tserkovnyak, G. Beach, E. Fullerton, C. Leighton, A. MacDonald, D. Ralph, D. Arena, H. Dürr, P. Fischer, J. Grollier, J. Heremans, T. Jungwirth, A. Kimmel, B. Koopmans, I. Krivorotov, S. May, A. Petford-Long, J. Rondinelli, N. Samarth, I. Schuller, A. Slavin, M. Stiles, O. Tchernyshyov, A. Thiaville, and B. Zink, Interface-induced phenomena in magnetism, Rev. Mod. Phys. **89**, 025006 (2017).

[17] G. Finocchio, F. Büttner, R. Tomasello, M. Carpentieri, and M. Kläui, Magnetic skyrmions: From fundamental to applications, J. Phys. D: Appl. Phys. **49**, 423001 (2016).

[18] W. Kang, Y. Q. Huang, X. C. Zhang, Y. Zhou, and W. S. Zhao, Skyrmion-electronics: An overview and outlook, Proc. IEEE **104**, 2040 (2016).

[19] G. Q. Yu, P. Upadhyaya, X. Li, W. Y. Li, S. K. Kim, Y. B. Fan, K. L. Wong, Y. Tserkovnyak, P. K. Amiri, and K. L. Wang, Room-temperature creation and spin orbit torque manipulation of skyrmions in thin films with engineered asymmetry, Nano Lett. **16**, 1981 (2016).

[20] K. Everschor-Sitte, J. Masell, R. M. Reeve, and M. Klaui, Perspective: Magnetic skyrmions-Overview of recent progress in an active research field, J. Appl. Phys. **124**, 240901 (2018).

[21] T. Moriya, Anisotropic superexchange interaction and weak ferromagnetism, Phys. Rev. **120**, 91 (1960).

[22] I. E. Dzyaloshinskii, Theory of helicoidal structures in antiferromagnets, JETP Lett. **19**, 960 (1964).

[23] M. Bode, M. Heide, K. von Bergmann, P. Ferriani, S. Heinze, G. Bihlmayer, A. Kubetzka, O. Pietzsch, S. Blugel, and R. Wiesendanger, Chiral magnetic order at surfaces driven by inversion asymmetry, Nature (London) **447**, 190 (2007).

[24] G. Chen, J. Zhu, A. Quesada, J. Li, A. T. N'Diaye, Y. Huo, T. P. Ma, Y. Chen, H. Y. Kwon, C. Won, Z. Q. Qiu, A. K. Schmid, and Y. Z. Wu, Novel Chiral Magnetic Domain Wall Structure in Fe/Ni/Cu(001) Films, Phys. Rev. Lett. **110**, 177204 (2013).

[25] M. Heide, G. Bihlmayer, and S. Blügel, Dzyaloshinskii-Moriya interaction accounting for the orientation of magnetic domains in ultrathin films: Fe/W(110). Phys. Rev. B **78**, 140403(R) (2008).

[26] A. Fert, V. Cros, and J. Sampaio, Skyrmions on the track, Nat. Nanotechnol. **8**, 152 (2013).

[27] J. Sampaio, V. Cros, S. Rohart, A. Thiaville, and A. Fert, Nucleation, stability and current-induced motion of isolated magnetic skyrmions in nanostructures, Nat. Nanotechnol. **8**, 839 (2013).

[28] X. C. Zhang, G. P. Zhao, H. Fangohr, J. P. Liu, W. X. Xia, J. Xia, and F. J. Morvan, Skyrmion-skyrmion and skyrmion-edge repulsions in skyrmion-based racetrack memory, Sci. Rep. **5**, 7643 (2015).

[29] X. Zhang, Y. Zhou, and E. Motohiko, Magnetic bilayer-skyrmions without skyrmion Hall effect, Nat. Commun. **7**, 10293 (2016).

[30] R. Tomasello, E. Martinez, R. Zivieri, L. Torres, M. Carpentieri, and G. Finocchio, A strategy for the design of skyrmion racetrack memories, Sci. Rep. **4**, 6784 (2014).

[31] G. Yu, P. Upadhyaya, Q. Shao, H. Wu, G. Yin, X. Li, C. He, W. Jiang, X. Han, P. K. Amiri, and K. L. Wang, Room-temperature skyrmion shift device for memory application, Nano Lett. **17**, 261 (2017).

[32] S. Woo, K. M. Song, X. Zhang, Y. Zhou, M. Ezawa, S. Finizio, J. Raabe, J. W. Choi, B.-C. Min, H. C. Koo, and J. Chang, Current-driven dynamics and inhibition of the skyrmion Hall effect of ferrimagnetic skyrmions in GdFeCo films, Nat. Commun. **9**, 959 (2018).

[33] N. Romming, C. Hanneken, M. Menzel, J. E. Bickel, B. Wolter, K. von Bergmann, A. Kubetzka, and R. Wiesendanger, Writing and deleting single magnetic skyrmions, Science **341**, 636 (2013).

[34] M. He, L. C. Peng, Z. Z. Zhu, G. Li, J. W. Cai, J. Q. Li, H. X. Wei, L. Gu, S. G. Wang, T. Y. Zhao, B. G. Shen, and Y. Zhang, Realization of zero-field skyrmions with high-density via electromagnetic manipulation in Pt/Co/Ta multilayers, Appl. Phys. Lett. **111**, 202403 (2017).

[35] W. Koshibae and N. Nagaosa, Creation of skyrmions and antiskyrmions by local heating, Nat. Commun. **5**, 5148 (2014).

[36] M. Finazzi, M. Savoini, A. R. Khorsand, A. Tsukamoto, A. Itoh, L. Duo, A. Kirilyuk, T. Rasing, and M. Ezawa, Laser-Induced Magnetic Nanostructures with Tunable Topological Properties, Phys. Rev. Lett. **110**, 177205 (2013).

[37] S. G. Je, P. Vallobra, T. Srivastava, J. C. Rojas-Sanchez, T. H. Pham, M. Hehn, G. Malinowski, C. Baraduc, S. Auffret, G. Gaudin, S. Mangin, H. Bea, and O. Boulle, Creation of magnetic skyrmion bubble lattices by ultrafast laser in ultrathin films, Nano Lett. **18**, 7362 (2018).

[38] M. Schott, A. Bernand-Mantel, L. Ranno, S. Pizzini, J. Vogel, H. Bea, C. Baraduc, S. Auffret, G. Gaudin, and D. Givord, The skyrmion switch: Turning magnetic skyrmion off with an electric field, Nano Lett. **17**, 3006 (2017).

[39] C. Ma, X. C. Zhang, J. Xia, M. Ezawa, W. J. Jiang, T. Ono, S. N. Piramanayagam, A. Morisako, Y. Zhou, and X. X. Liu, Electric field-induced creation and directional motion of domain walls and skyrmion bubbles, Nano Lett. **19**, 353 (2019).

[40] J. Iwasaki, M. Mochizuki, and N. Nagaosa, Current-induced skyrmion dynamics in constricted geometries, Nat. Nanotechnol. **8**, 742 (2013).

[41] Y. Zhou and M. Ezawa, A reversible conversion between a skyrmion and a domain-wall pair in a junction geometry, Nat. Commun. **5**, 4652 (2014).

[42] S.-Z. Lin, Edge instability in a chiral stripe domain under an electric current and skyrmion generation, Phys. Rev. B **94**, 020402(R) (2016).

[43] F. Büttner, I. Lemesh, M. Schneider, B. Pfau, C. M. Gunther, P. Hessing, J. Geilhufe, L. Caretta, D. Engel, B. Kruger, J. Viefhaus, S. Eisebitt, and G. S. D. Beach, Field-free deterministic ultrafast creation of magnetic skyrmions by spin-orbit torques, Nat. Nanotechnol. **12**, 1040 (2017).

[44] A. Hrabec, J. Sampaio, M. Belmeguenai, I. Gross, R. Weil, S. M. Chérif, A. Stachkevitch, V. Jacques, A. Thiaville, and S. Rohart, Current-induced skyrmion generation and dynamics in symmetric bilayers, Nat. Commun. **8**, 15765 (2017).

[45] W. Legrand, D. Maccariello, N. Reyren, K. Garcia, C. Moutafis, C. Moreau-Luchaire, S. Collin, K. Bouzehouane, V. Cros, and A. Fert, Room-temperature current-induced generation and motion of sub-100nm skyrmions, Nano Lett. **17**, 2703 (2017).

[46] O. Heinonen, W. Jiang, H. Somaily, S. G. E. te Velthuis, and A. Hoffmann, Generation of magnetic skyrmion bubbles by inhomogeneous spin Hall currents, Phys. Rev. B **93**, 094407 (2016).

[47] W. Jiang, W. Zhang, G. Q. Yu, M. B. Jungfleisch, P. Upadhyaya, H. Somaily, J. E. Pearson, Y. Tserkovnyak, K. L. Wang, O. Heinonen, S. G. E. te Velthuis, and A. Hoffmann, Mobile Neel skyrmions at room temperature: status and future, AIP Adv. **6**, 055602 (2016).

[48] K. Everschor-Sitte, M. Sitte, T. Valet, A. Abanov, and J. Sinova, Skyrmion production on demand by homogeneous DC currents, New J. Phys. **19**, 092001 (2017).

[49] M. Ezawa, Giant Skyrmions Stabilized by Dipole-Dipole Interactions in Thin Ferromagnetic Films, Phys. Rev. Lett. **105**, 197202 (2010).

[50] K. Everschor-Sitte and M. Sitte, Real-space Berry phases: Skyrmion soccer (invited). J. Appl. Phys. **115**, 172602 (2014).

[51] G. B. Liu, D. Li, P. F. de Chatel, J. Wang, W. Liu, and Z. D. Zhang, Control of Hall angle of Skyrmion driven by electric current, Chin. Phys B **25**, 067203 (2016).

[52] S. Luo, M. Song, X. Li, Y. Zhang, J. Hong, X. Yang, X. Zou, N. Xu, and L. You, Reconfigurable skyrmion logic gates, Nano Lett **18**, 1180 (2018).

[53] C. Reichhardt, D. Ray, and C. J. O. Reichhardt, Collective Transport Properties of Driven Skyrmions with Random Disorder, Phys. Rev. Lett. **114**, 217202 (2015).

[54] A. Hoffmann, Spin Hall effects in metals, IEEE Trans. Magn. **49**, 5172 (2013).

[55] J. Sinova, S. O. Valenzuela, J. Wunderlich, C. H. Back, and T. Jungwirth, Spin Hall effects, Rev. Mod. Phys. **87**, 1213 (2015).

[56] L. Q. Liu, C. F. Pai, Y. Li, H. W. Tseng, D. C. Ralph, and R. A. Buhrman, Spin-torque switching with the giant spin Hall effect of tantalum, Science **336**, 555 (2012).

[57] K. Ueda, K.-J. Kim, Y. Yoshimura, R. Hiramatsu, T. Moriyama, D. Chiba, H. Tanigawa, T. Suzuki, E. Kariyada, and T. Ono, Transition in mechanism for current-driven magnetic domain wall dynamics, Appl. Phys. Express. **7**, 053006 (2014).

[58] M. J. Donahue and D. G. Porter, OOMMF *User's Guide* (Interagency Report NISTIR 6376, NIST, Gaithersburg, MD, http://math.nist.gov/oommf (1999).

[59] See Supplemental Material at http://link.aps.org/supplemental/10.1103/PhysRevB.100.184426, for detailed discussion about the micromagnetic simulation and solution of Thiele equation in the presence of inhomogeneous currents, and Refs. [30,66].

[60] W. Koshibae and N. Nagaosa, Theory of antiskyrmions in magnets, Nat. Commun. **7**, 10542 (2016).

[61] M. Hoffmann, B. Zimmermann, G. P. Müller, D. Schürhoff, N. S. Kiselev, C. Melcher, and S. Blügel, Antiskyrmions stabilized at interfaces by anisotropic Dzyaloshinskii-Moriya interactions, Nat. Commun. **8**, 308 (2017).

[62] M. Stier, W. Hausler, T. Posske, G. Gurski, and M. Thorwart, Skyrmion-Anti-Skyrmion Pair Creation by In-Plane Currents, Phys. Rev. Lett. **118**, 267203 (2017).

[63] X. Zhang, J. Xia, Y. Zhou, X. Liu, H. Zhang, and M. Ezawa, Skyrmion dynamics in a frustrated ferromagnetic film and current-induced helicity locking-unlocking transition, Nat. Commun. **8**, 1717 (2017).

[64] Y. Liu, H. Yan, M. Jia, H. F. Du, and A. Du, Topological analysis of spin-torque driven magnetic skyrmion formation, Appl. Phys. Lett. **109**, 102402 (2016).

[65] C. Reichhardt and C. J. O. Reichhardt, Magnus-induced dynamics of driven skyrmions on a quasi-one-dimensional periodic substrate, Phys. Rev. B **94**, 094413 (2016).

[66] A. A. Thiele, Steady-State Motion of Magnetic Domains, Phys. Rev. Lett. **30**, 230 (1973).

[67] R. Tomasello, A. Giordano, S. Chiappini, R. Zivieri, G. Siracusano, V. Puliafito, I. Medlej, A. La Corte, B. Azzerboni, M. Carpentieri, Z. M. Zeng, and G. Finocchio, Micromagnetic understanding of the skyrmion Hall angle current dependence in perpendicularly magnetized ferromagnets, Phys. Rev. B **98**, 224418 (2018).